Title

Exploring new roles for actin upon LTP induction in dendritic spines

Journal

Scientific Reports, 11(1)

ISSN

2045-2322

Authors

Bonilla-Quintana, Mayte

Wörgötter, Florentin

Publication Date

2021

DOI

10.1038/s41598-021-86367-z

Peer reviewed

scientific reports

Check for updates

OPEN

Exploring new roles for actin upon LTP induction in dendritic spines

Mayte Bonilla-Quintana[1,2]✉ & Florentin Wörgötter[1]

Dendritic spines, small protrusions of the dendrites, enlarge upon LTP induction, linking morphological and functional properties. Although the role of actin in spine enlargement has been well studied, little is known about its relationship with mechanical membrane properties, such as membrane tension, which is involved in many cell processes, like exocytosis. Here, we use a 3D model of the dendritic spine to investigate how polymerization of actin filaments can effectively elevate the membrane tension to trigger exocytosis in a domain close to the tip of the spine. Moreover, we show that the same pool of actin promotes full membrane fusion after exocytosis and spine stabilization.

Dendritic spines are small protrusions from the dendrites where the postsynaptic part of most excitatory synapses are located. At the tip of the spines and opposite to the presynaptic bouton, there is a specialized substructure called the postsynaptic density (PSD) where receptors and signalling molecules are localized. The AMPA-type glutamate receptors (AMPARs) in the PSD are activated when the presynaptic neuron releases glutamate. The spine depolarizes when these receptors are strongly activated, allowing calcium (Ca^{2+}) entry via *N*-methyl-**D**-aspartate receptors (NMDARs). This triggers an increase in spine size that is associated with an increase in AMPA-receptor-mediated currents and depends on NMDARs, calmodulin, and actin polymerization[1]. Such an increase in AMPA-receptor-mediated current is due to an increment of AMPARs at the synapse by exocytosis or lateral movement[2,3]. Moreover, it enhances the signal transmission between two neurons, thereby strengthening their synapse in a process called long-term potentiation (LTP, see Fig. 1 for a schematic description). These activity-dependent structural modifications of dendritic spines are thought to be the cellular basis for learning and memory[1].

The size increase of the spines after stimulation (i.e., Ca^{2+} entry via NMDARs) is $\approx$ 200% of their initial volume within 5 min[1,4,5]. In some spines, volume increments of $\approx$ 50% have been observed after 100 min of initial stimulation[1], indicating that the initial increase of spine volume after stimulation is transient and that spine volume stabilizes at a smaller value, that is still larger than the initial value. This volume change is possible due to actin, the principal cytoskeleton component in the spine[4]. Actin is a globular protein (G-actin) that assembles into filaments (F-actin), which are polar structures that undergo a continuous treadmilling process, where G-actin with bound ATP is polymerized at the barbed (+) end of the filament. The bounded ATP hydrolyzes to ADP promoting depolymerization of G-actin at the pointed (−) end of the filament. Actin binding proteins (ABPs) promote polymerization and depolymerization, as well as branching and severing of F-actin.

Within spines, there is a dynamic equilibrium between G- and F-actin[6] that results in continuous shape fluctuations[7] observed in basal conditions (without induction of LTP). Moreover, actin filaments are organized in two different pools: a dynamic pool localized at the tip of the spine with fast treadmilling velocity ($\approx$ 40 s), and a static pool with slow treadmilling velocity ($\approx$ 17 min) at the base of the spine head[8]. Frost et al.[9] observed that the fast treadmilling actin mostly localizes in discrete well-separated foci at the tip of the spine. In Bonilla-Quintana et al.[10], we showed how the continuous shape fluctuations of dendritic spines result from a continuous nucleation and vanishing of these foci. After LTP induction, a third pool, called the "enlargement" pool, forms[8]. According to Honkura et al.[8], this pool of actin is different to the dynamic and static pool because it requires calmodulin activation and has a treadmilling velocity of 2–15 min. Moreover, it is necessary for long-lasting spine enlargement. Importantly, actin serves as the main anchoring site for many postsynaptic proteins including NMDA and AMPA receptors[11]. Interestingly, the PSD size correlates with spine size and the PSD grows in spines that show persistent enlargement[12].

Upon LTP, the structural changes in spines can be divided into three temporal phases[5]. During the first phase (1–7 min), spines rapidly expand due to an increase in the concentration of ABPs, such as Arp2/3 and Aip1, that modify F-actin through severing, branching and capping. At the same time, the pool of ABPs, which

[1]University of Göttingen, Göttingen, Germany. [2]University of California, San Diego, USA. ✉email: mbonillaquintana@ucsd.edu

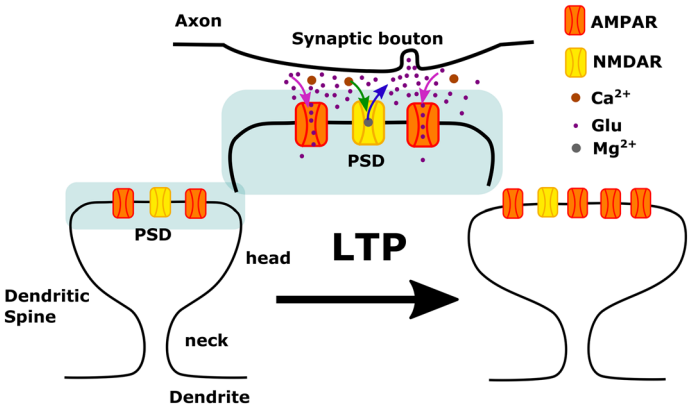

Figure 1. Long-Term Potentiation (LTP) in dendritic spines. AMPA receptors (orange) located at the postsynaptic density (PSD) in mature dendritic spines (left) are activated (magenta arrows) by Glutamate (Glu, purple circles) released from the synaptic bouton in the axon of the presynaptic neuron. When the AMPA receptors are strongly stimulated, the postsynaptic cell is depolarized causing the release (blue arrow) of the Magnesium ion (Mg^2, gray circle) that blocks the NMDA receptor (yellow), allowing the entry of calcium (Ca^{2+}, brown circles) to the spine. This process is known as LTP induction (middle) and triggers an increase of spine size and the number of AMPA receptors (right). In this study we specifically address the actin processes that result from LTP induction and lead to spine increase, exocytosis of AMPARs and spine stabilization.

stabilizes F-actin, is transiently depleted. Thus, during this phase there is an increase in actin polymerization at the barbed ends that elongates F-actin, promoted by F-actin severing, resulting in a profound remodelling of the spine. During the second phase (7–60 min) ABPs that modify F-actin and ABPs that promote F-actin stabilization return to their basal levels, thereby stabilizing the F-actin cytoskeleton. In the third phase (> 60 min), the concentration of some PSD proteins within the spine increases. These proteins are translocated to the PSD, which results in PSD enlargement, thereby, recovering the relation between spine and PSD size (see Fig. 5). Note, however, that some studies also show that different PSD proteins experience an almost immediate increase in their concentration upon LTP[12].

Actin polymerization at the barbed ends near the membrane generates a force that pushes the membrane forward[13] and raises the membrane tension locally[14], which is involved in many cell processes. For example, it controls cell motility by producing the signal that coordinates membrane trafficking (via exocytosis), actomyosin contraction, and plasma membrane area change[15]. Moreover, the membrane tension generated by F-actin polymerization facilitates shrinking of the fusion-generated Ω-profile during exocytotic events[16]. Previous 3D models of fibrolasts exhibit how the membrane physical forces control cell shape during spreading[17,18], and a recent theoretical model shows that membrane tension is important for maintenance of different spines shapes[19]. However, to our knowledge, the effects of spine enlargement after induction of LTP on membrane tension and its consequences in cellular processes, such as exocytosis, have been neglected both experimentally and theoretically.

Here, we extend our theoretical model[10] to investigate the roles of actin polymerization upon LTP in 3D. For this we now measure the force generated by membrane tension at different tracking points and simulate the Ω -profile merging and PSD growth. Assuming that an increase in membrane tension acts as a mechanical signal that triggers exocytosis, we examine how actin polymerization induces such an increase by simulating different scenarios. Moreover, we study how actin facilitates membrane fusion during exocytosis and size stabilization. We find that a single F-actin polymerization focus located near the PSD increases membrane tension most efficiently and aids membrane fusion and spine stabilization, suggesting that these events co-localize and result from a continuous reorganization of actin in this focus.

Results

We used a theoretical model, based on Bonilla-Quintana et al.[10], in which asymmetric spine shape changes result from an imbalance between a force generated by actin polymerization, that pushes the membrane forward, and the membrane force that counteracts these deformations. To allow for a better measure of the membrane tension, we used a simplified description of the actin dynamics that characterizes the force generated by polymerization at the barbed ends, instead of modeling a single filament treadmilling process with its branching and severing events. Moreover, we only considered the actin that is polymerizing close to the spine membrane and, thus, affects its shape.

Distribution of F-actin polymerization affects the force generated by membrane tension. In the absence of external forces, our modeled spine membrane reaches a resting shape that minimizes the membrane energy ($\mathcal{E}_{mem}$ in Eq. (4), black shape in Fig. 2a). After obtaining the resting shape for a spine, considering experimental data of spine size and PSD surface area[12,20] (see "Methods" for details), we simulated LTP induction by including a force generated by rapid and persistent F-actin polymerization[6]. This corresponds to the first phase of the structural changes in the spine triggered by LTP induction where actin filaments are continuously

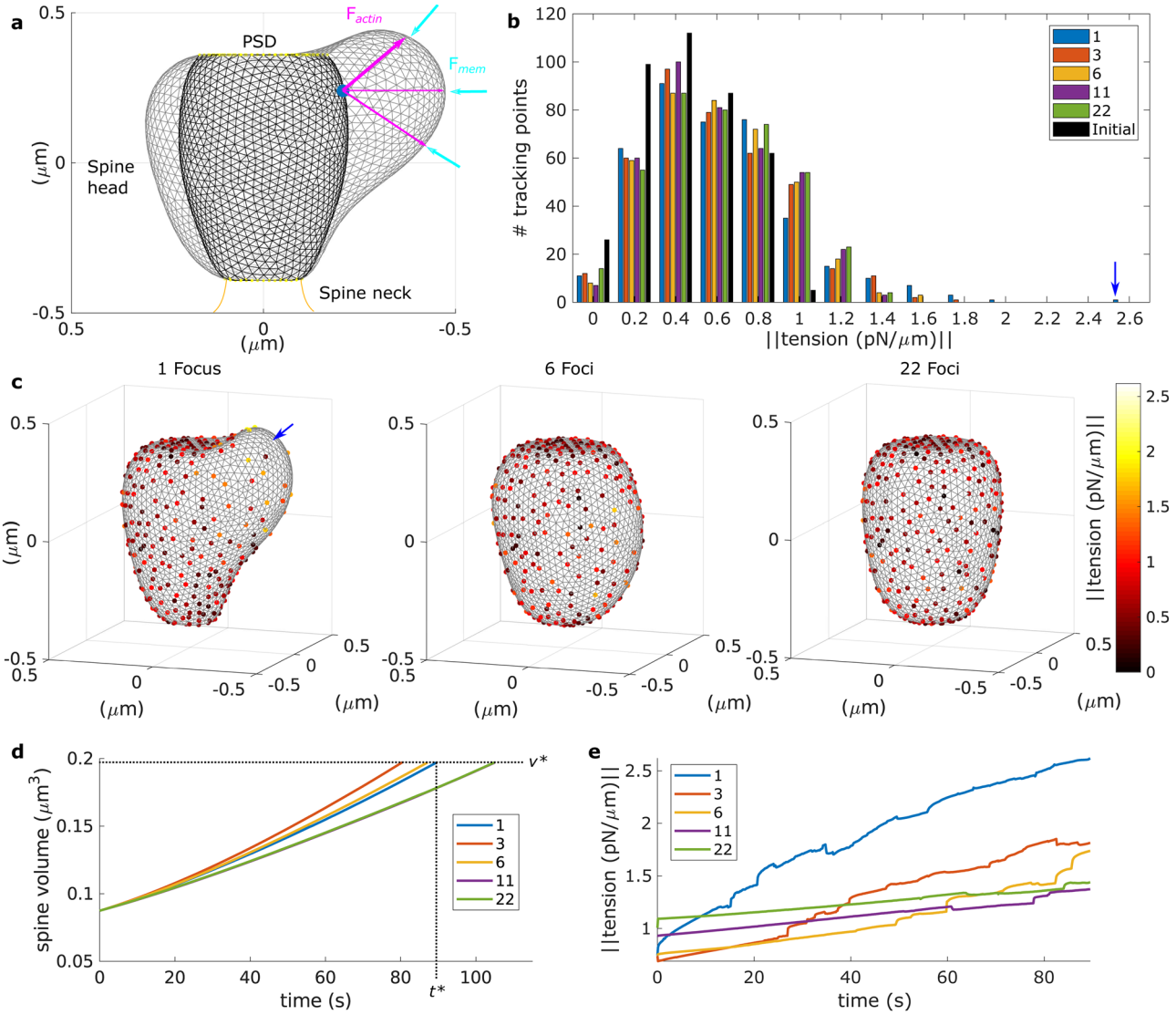

Figure 2. Spine enlargement upon LTP for different number of F-actin polymerization foci. (**a**) Spine resting shape (black), and spine shape after LTP induction (gray, corresponding to the shape in (**c**) with 1 Focus). The blue dot signals the location of the F-actin polymerization focus. Note that the shape in gray represents a deformation of that in black, which arises from the interplay between the force generated by F-actin polymerization ($\mathbf{F}_{actin}$, magenta arrows) and the counteracting force of the membrane ($\mathbf{F}_{mem}$, cyan arrows) in response to this deformation. This plot shows the $y-z$ axis for $x=0$. (**b**) Histogram of the distribution of the force generated by membrane tension measured at the tracking points when the spines reach a volume equal to v^*. Colors denote the number of polymerization foci distributed in the spine for each simulation. The distribution of the membrane tension for the resting shape, used at the beginning of the simulations, is shown in black. Blue arrow signals maximum tension. The skewness of the distributions is 1.0807 (1 focus), 0.5510 (3 foci), 0.3863 (6 foci), 0.3157 (11 foci), 0.2019 (22 foci) and 0.0955 (resting shape). (**c**) Spines shapes (gray) at time t^* with different number of F-actin polymerization foci. Dots are the tracking points color-coded for the force generated by the membrane tension. The polymerization foci are evenly distributed along the spine but are not plotted in these figures to avoid confusion with the tracking points. (**d**) Spine volume evolution over time, color-coded by the number of polymerization foci. Note that the traces for 11 and 22 foci are very similar. Dotted black lines denote t^* and v^*. (**e**) Evolution of the membrane tension for the tracking point with maximum membrane tension when the spine reaches a volume v^*.

assembled and disassembled[4] (see Fig. 5). In our model, this is simulated by a continuous force $\mathbf{F}_{actin}$, given by Eq. (2), that pushes the membrane forward and is inversely proportional to the distance between the starting (nucleation) location of the F-actin polymerization focus $\mathbf{f}^i$ and the spine membrane. Thus, the actin polymerization force is greater near the nucleation location and diminishes as the spine expands.

This actin force description is based on the work of Mogilner and Edelstein-Keshet[21]. In short, they observed that when the number of barbed ends is large in the lamellipodial protrusion of a cell, G-actin is depleted, causing a decrease in the protrusion velocity, which is inversely proportional to the number of barbed ends. Here,

we assumed that the number of barbed ends increases after LTP induction, mostly due to a continuous F-actin branching and severing. Due to branching, the F-actin spatially spreads, but as the spine grows, the availability of G-actin for polymerizing is reduced and the protrusion velocity decreases. Our proposed actin force captures this phenomenon (see Supplementary Fig. S1).

When the membrane deforms due to the actin polymerization force, its energy increases and generates a response force $\mathbf{F}_{mem}$ (Eq. (3)). Figure 2a shows the resulting spine shape in gray. In our simulations, we tracked $\mathbf{F}_{mem}$ and each of its components at different locations along the spine membrane, in particular the work needed to increase the surface area (dots in Fig. 2c). This way, we captured the membrane force generated by tension (tension force) and studied its spatial distribution and evolution over time and whether it depends on the number of actin foci. This method to approximate the membrane tension force resembles experiments that use optical tweezers to calculate tether force[15] in the sense that both obtain the force generated by the displacement of a reference point. In Gauthier et al.[15] the membrane tension is proportional to the square of the tether force, but here we did not attempt to calculate this relationship and, instead, reported the tension force derived from Eq. (3). During these simulations, the PSD and neck size remained unchanged (yellow dots in Fig. 2a), as observed in experiments within this temporal interval[4,5,12].

First, we investigated spine expansion and membrane tension force under different scenarios of F-actin polymerization locations upon LTP induction, namely, an actin polymerization focus located near to the PSD and various actin polymerization focus evenly distributed within the spine head. To allow comparison between these scenarios, $\mathbf{F}_{actin}$ (Eq. 2) was multiplied by a constant ϕ, that is inversely proportional to the number of polymerization foci. Thus, the force generated by actin polymerization was distributed among the foci.

We found that when actin polymerization accumulates in one location near to the PSD, the membrane tension force increased 2.5-fold at that location at time $t^* = 89.5$ s. Thereupon, the spine volume is $v^* = 0.1970\ \mathrm{m}\mu^3$, growing by $\approx 125\%$. Spines with more F-actin polymerization foci also increased their volume to v^*, but at different times (Fig. 2d). Because $\mathbf{F}_{actin}$ distributes among the polymerization foci, the time difference to reach the same volume is related to the foci position within the spine. When there are many foci within the spine (11 or 22), the spine volume increases similarly, as shown by the purple and green traces in Fig. 2d. If there are few foci, two of them could be close enough to cooperate, resulting in a fast enlargement, as in the case with 3 foci. This highlights the complex interaction between $\mathbf{F}_{mem}$ and $\mathbf{F}_{actin}$ in our model that emerges from the spine morphology.

Figure 2c shows spines at t^* for different number of foci. Note that spines with more foci increased their volume and the force generated by the membrane tension more isotropic. The histogram of this force, measured by the tracking points when they reach a volume of v^* (Fig. 2b), reveals that only in the spine with one focus it is greater than 2 pN. Moreover, Fig. 2e shows that the evolution of the membrane tension force over time, measured at the tracking point with the maximum tension force value at v^*, is lower for spines with more than one focus.

When studying the evolution of the distribution of the tension force among the tracking points, we observed that at the start of the simulation 60.61% of the tracking points measured a force less than 0.6 pN (black bars in Fig. 2b). After t^* only 42.46% of the points in the spine with one focus measured less than 0.6 pN (blue bars in Fig. 2b). Thus, the tension force increases at most locations and has a total increase from 210.6736 pN, at the start of the simulation, to 280.6355 pN at t^*. Spines with more foci also increase the measured tension force at the tracking locations, but the resulting distribution resembles a normal distribution whilst the distribution of the spine with one focus is skewed. Moreover, the sum of the tension force measured at the spines with more than one focus when they reached a volume of v^*, is less of that of the spine with one focus (272.71 pN, 275.1510 pN, 274.6277 pN, 278.8661 pN for spines with 3, 6, 11 and 22 foci, respectively).

We conclude that after LTP induction, the force generated by membrane tension shows a bigger increase when F-actin polymerization concentrates in a specific location than when it is evenly distributed over the spine. This is because the spine with one focus experiences a greater deformation due to actin polymerization than the evenly distributed size increase of the spines with more foci. Importantly, this is not an effect of the dependency of the number of foci on the parameter ϕ of Eq. (2), as exhibited in Supplementary Fig. S2, which shows the evolution of a spine with one or 22 foci with the same value of ϕ. Since membrane tension serves as a mechanical signal for exocytosis[15] and the force generated by the membrane tension is proportional to the membrane tension, these results are in line with experimental observations of a defined exocytic domain in the spine[22].

Position of the F-actin polymerization focus affects membrane tension. Next, we investigated whether the location of the polymerization focus affects the force generated by membrane tension. We compared the spine shape resulting from the polymerization focus near the PSD (Fig. 2a) with those having the focus in the middle of the spine head or near the spine neck. Figure 3a shows that the spine shapes are different when they reached a volume of v^*, albeit having the same volume. Spines with the polymerization focus far from the PSD reached this volume faster (Fig. 3c). However, Fig. 3b shows that, when the spines reach a volume of v^*, the maximum tension force, measured by the tracking points, is higher for the spine with the focus near to the PSD. Moreover, the sum of these forces along the tracking points is also higher in such a spine (280.6355 pN, compared to 275.1624 pN and 278.7298 pN in the spine with the focus in the middle and near the neck, respectively). Likewise, the evolution of the tension force, measured at the tracking points corresponding to the highest tension force in the spines with volume v^*, shows higher values for the spine with the polymerization focus near to the PSD (Fig. 3d). Importantly, these results hold for different randomly allocated polymerization focus in these different regions (Supplementary Fig. S3) and for different number of tracking points (Supplementary Fig. S4).

Note that when the polymerization focus is near the PSD, the membrane stretches more due to the PSD immobility. Although the neck was also fixed, the effect on the force generated by the membrane tension was lower because the neck surface area is smaller. Taking everything together, the force generated by the membrane

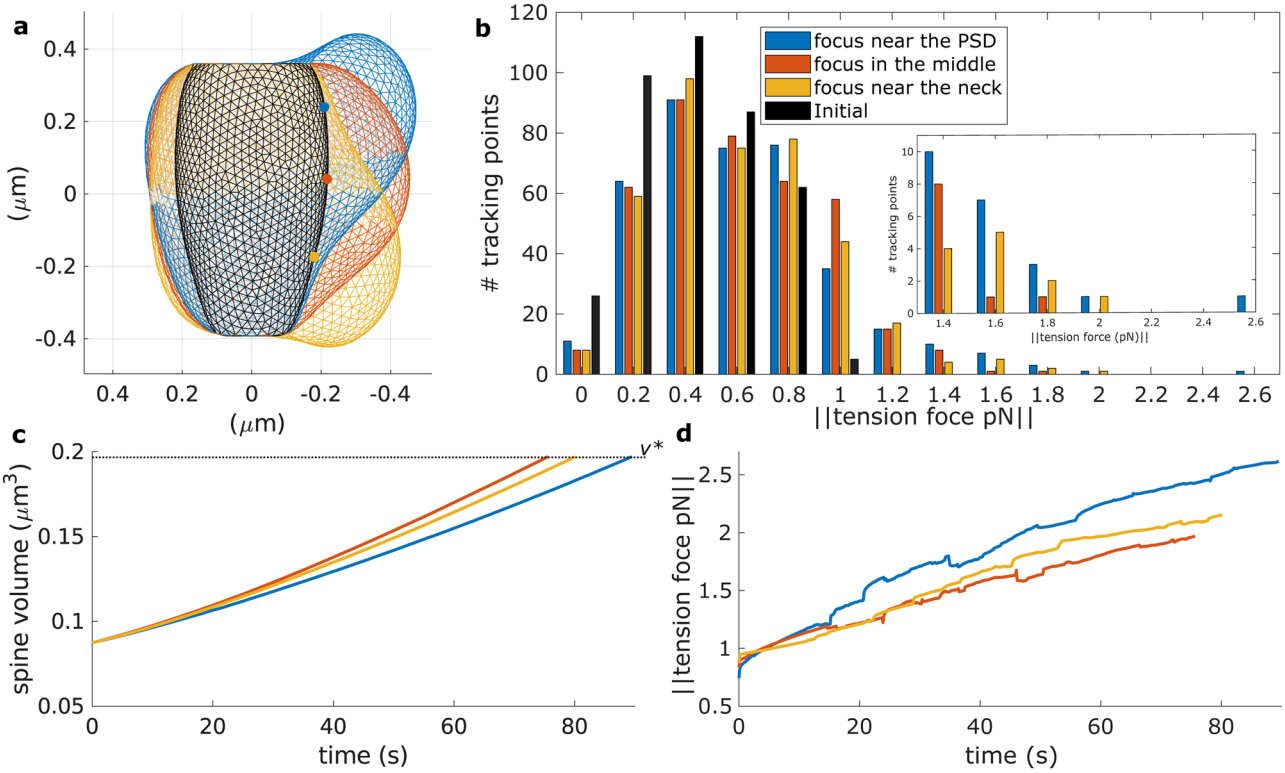

Figure 3. Spine enlargement upon LTP for different locations of the F-actin polymerization focus. (**a**) Spine shapes for different locations of the F-actin polymerization focus (dots) when they reached a volume of v^* (this occur at different times, see (**c**)), color-coded as in (**b**). This plot shows the $y-z$ axis, for $x=0$. (**b**) Histogram of the distribution of the force generated by membrane tension measured at the tracking points when the spines reached a volume of v^*. (**c**) Spine volume evolution over time, color-coded by the number of polymerization foci. Dotted black line denotes v^*. (**d**) The evolution of the membrane tension for the tracking point with maximum membrane tension when the spine reaches a volume of v^*.

tension reaches a higher value when the F-actin polymerization focus is near the PSD, indicating that the exocytotic domain locates therein, as observed in Kennedy et al.[22].

F-actin polymerization promotes membrane fusion upon exocytosis. We have shown in our model that when F-actin polymerization concentrates at a certain location near the PSD, it rapidly elevates the force generated by the membrane tension, which can serve as a signal for exocytosis[15]. In the spine, exocytosis is important for increase of AMPARs at the PSD and membrane trafficking after LTP induction[2,22,23]. To achieve membrane fusion and cargo release, vesicles dock to the membrane and form an Ω-shaped structure[16] that has to shrink and merge with the membrane. In our model, shape deformations, like the Ω-profile, generate a response force in the membrane $\mathbf{F}_{mem}$ that restores it to the resting shape. However, Wen et al.[16] showed that F-actin polymerization mediates Ω-profile merging. Therefore, we investigated two scenarios for Ω-profile shrinking, namely, shrinking resulting only from $\mathbf{F}_{mem}$ dynamics and shrinking aided by F-actin polymerization. For this, we imposed a deformation to the modeled spine to resemble the Ω-profile formed for a recycling vesicle with diameter ≈ 0.125 μm, corresponding to experimental observations[16] (see "Methods" for details).

In the first scenario, we assumed that when exocytosis starts, myosin contracts and pulls the F-actin away from the membrane, as observed in Gauthier et al.[15]. Consequently, the force generated by actin polymerization ceases. Experimental data show that this is possible in spines since myosin II activates upon LTP induction and is required for stabilization of synaptic plasticity[24]. Therefore, we set $\mathbf{F}_{actin}=\mathbf{0}$ and observed that the Ω-profile depicted in Fig. 4a (highlighted in magenta) shrinks fully within 30 seconds (see yellow shapes in Fig. 4d), decreasing spine volume and surface area (Fig. 4b,c). However, exocytosis provides membrane to the spine for enlargement upon LTP[22,23]. Therefore, there must be an increase in surface area of the spine membrane.

Consequently, we considered a second scenario where actin filaments remain close to the membrane and polymerize. Hence, they generate a polymerization force (i.e. $\mathbf{F}_{actin}\neq\mathbf{0}$) from a focus at the tip of the Ω-profile (blue dot in Fig. 2a). Within 10 s, the spine membrane surface area returned to its initial value (Fig. 4c), indicating a possible full merge of the Ω-profile, which supplies membrane. The initial decrease in membrane surface area is transient and could be due the distribution of F-actin. Note that during the simulation, the spine volume increases (Fig. 4b) and the Ω-profile shrinks completely. To test whether the location of the actin focus affects the reduction of the Ω-profile, we ran a simulation with the polymerization focus located next it (orange dot in Fig. 4a). In this case, the volume and surface area of the spine increase (Fig. 4b,c), and the Ω-profile shrinks (Fig. 4d). However, the increase is less than for the previous case and the spine membrane is slightly pushed aside.

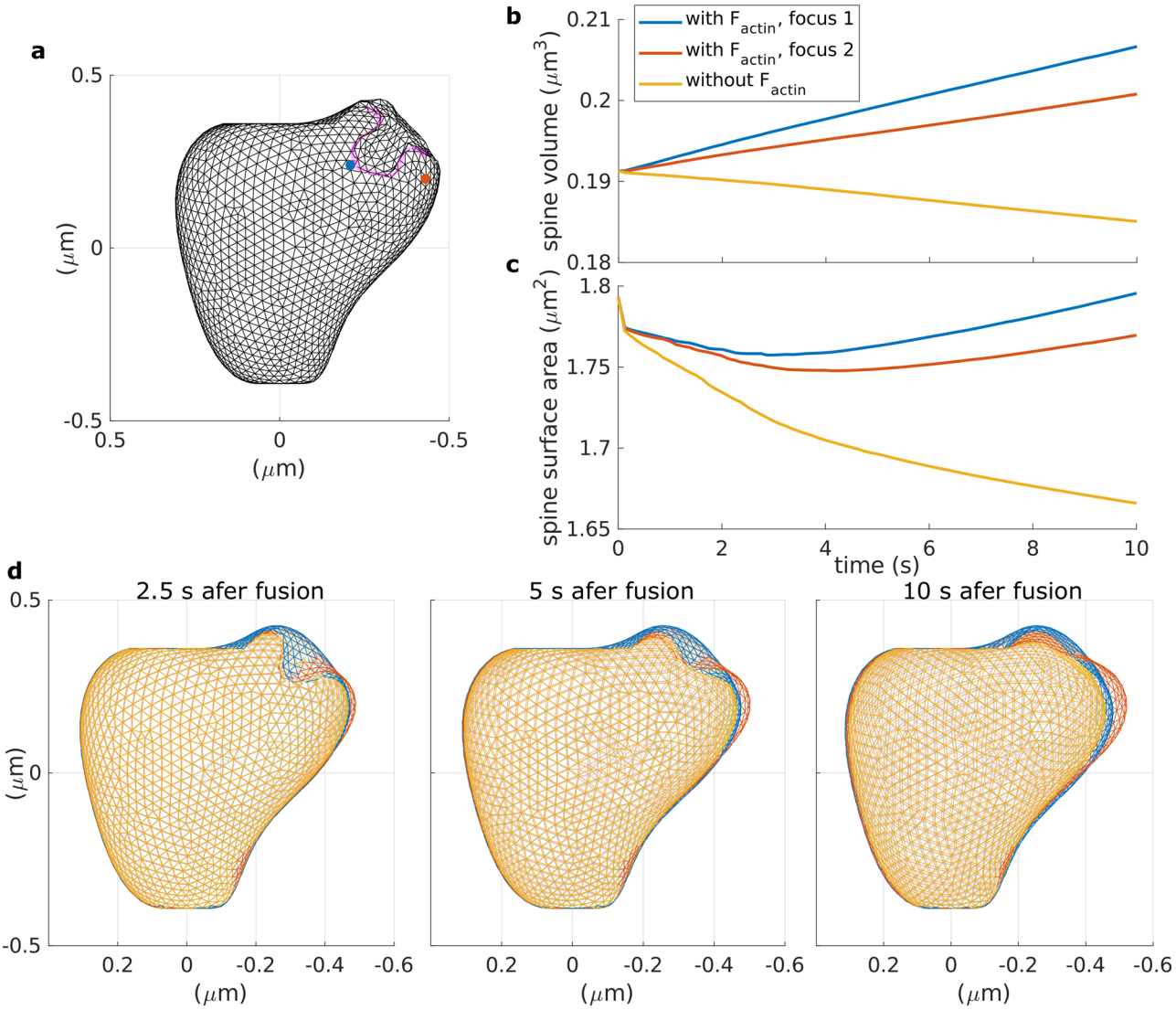

Figure 4. Exocytosis with and without the aid of F-actin polymerization. (**a**) Dendritic spine membrane after fusion with a recycling endosome. The invagination, highlighted in magenta, is the Ω-profile formed after the fusion event. The blue and orange dots represent the distinct F-actin polymerization foci. (**b**) Spine volume evolution over time, color-coded depending whether the Ω-profile merging is aided by $\mathbf{F}_{actin}$ or not. (**c**) Spine area surface evolution over time, color-coded as in (**b**). (**d**) Snapshots taken at different times after initiation of spine membrane fusion with the recycling endosome, color-coded as in (**b**).

These results suggest that actin polymerization is needed for membrane insertion resulting from the full merge of the Ω-profile formed upon exocytosis. Moreover, they indicate that the pool of F-actin that polymerizes and elevates the membrane tension to trigger exocytosis is involved in promoting Ω-profile shrinkage and the full fusion of the vesicle with the spine membrane. Hence, we speculated that there is a pool of F-actin that translocates to a focus near the PSD upon LTP and pushes the membrane forward elevating the force generated by the membrane tension to trigger exocytosis (see Fig. 5). Then, this same pool promotes the shrinkage of the Ω-profile generated when the vesicle docks to the membrane, and hence, full fusion.

Role of the F-actin polymerization focus for spine stabilization. Next, we studied whether the F-actin pool responsible for triggering and completing the exocytosis events, also accounts for spine stabilization. We hypothesized that after exocytosis, F-actin no longer polymerizes at a fast rate close to the spine membrane. This could be due to the contraction of F-actin promoted by myosin[15] or due to changes in ABPs, namely, an increase in proteins that promote F-actin stabilization and the switch in cofilin function: from severing F-actin to forming stable filaments[5].

In our simulations, we increased the radius of the PSD at a rate of Δ_{PSD} each time-step and stabilized the F-actin corresponding to spine enlargement within this radius by fixing it at a height of h_{PSD} (see "Methods"). Figure 6a,b shows the increase in the PSD surface area and the evolution of the spine volume from an initially expanded shape (similar to that in gray in Fig. 2a) for different values of Δ_{PSD}. Note that larger values of Δ_{PSD}

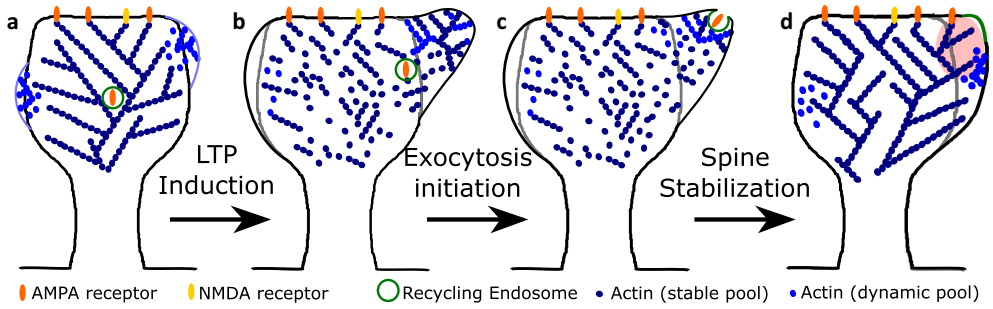

Figure 5. Actin re-organization upon LTP. (**a**) Before LTP induction, actin distributes in a stable and dynamic pool (dark and light blue dots, respectively). Spontaneous shape fluctuations (light blue lines) result from polymerization of the dynamic pool that organizes in distinct foci[9,10,25]. Note that only actin polymerizing close to the membrane can push the membrane forward. (**b**) ≈ 1 min after LTP induction, actin rapidly assembles and disassembles. Actin polymerizes at a single location near to the PSD, elevating the force generated by the membrane tension which triggers exocytosis of the recycling endosome. The initial spine shape is in gray. (**c**) Actin polymerization promotes full fusion of the Ω-profile formed after the docking of the recycling endosome with the spine membrane. (**d**) After completing exocytosis, the spine stabilizes. There is an increase in the AMPARs and spine size. Also, the membrane from the recycling endosome (in green) is merged with the spine membrane. Note that the spine enlargement occurs where the polymerization focus of (**a**) was located (highlighted in red).

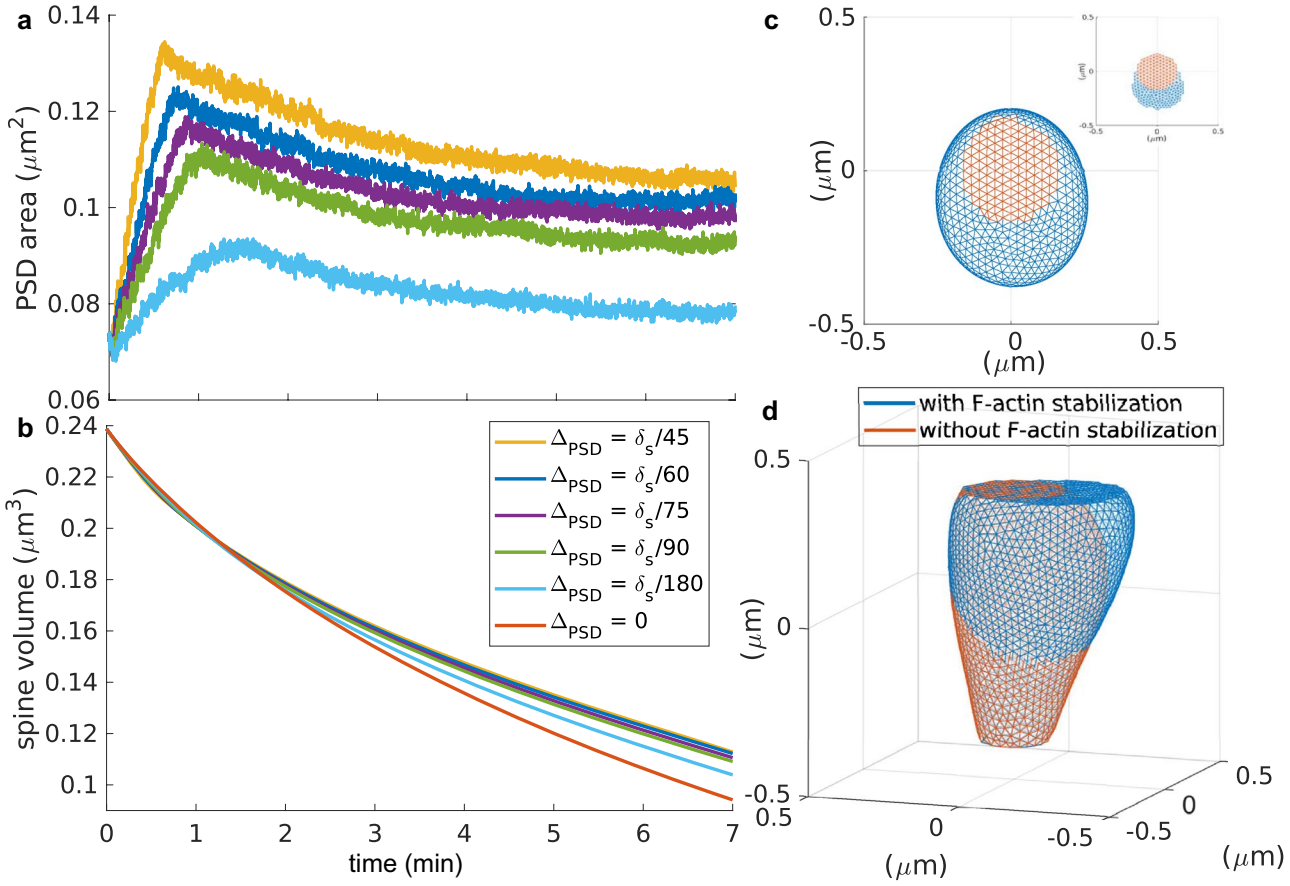

Figure 6. Stabilization of F-actin focus. (**a**) PSD surface area over time for different increments of Δ_{PSD}, color-coded as in (**b**). (**b**) Spine volume evolution over time for different increments of Δ_{PSD}. (**c**) Top view of a spine after 7 min of increasing the PSD size (blue, $\Delta_{PSD} = \delta_s/60$) and without changing the PSD (orange). Inset shows only the mesh corresponding to the PSD. (**d**) Front view of the spines in (**c**).

reach a higher maximum PSD surface area faster. However, eventually, the PSD surface area settles to a lower value that depends on Δ_{PSD}. Here, the fluctuations in the evolution are an artifact of the mesh approximation used for the membrane. We speculate that the decrease in the PSD area is a consequence of spine shrinkage due to the membrane force that moves the vertices corresponding to the enlarged PSD away from h_{PSD}.

Increasing the PSD area leads to an increase in spine volume, the higher Δ_{PSD} the bigger the spine (Fig. 6b). The difference between spines with and without the proposed F-actin stabilization is shown in Fig. 6c,d. After seven minutes, the spine without F-actin stabilization (in orange) reduces its initial volume by 60.56% whilst the spine with F-actin stabilization (in blue) decreases by 52.99% with a PSD increase of 42.87%. At this point, the proportion between spine head volume and PSD size, proposed by Arellano et al.[20], is kept: PSD size (0.1030 μm) $\approx 0.88 \times$ volume ($0.88 \times 0.1122\,\mu m^3 = 0.0987\,\mu m^3$).

Therefore, our simulations show that the F-actin promoting full membrane fusion in an exocytotic event can be stabilized and serve as anchoring place for PSD proteins. Although the stabilization of this pool of F-actin leads to a asymmetrical growth of the PSD, it does not perturb the shrinkage of the spine. We assumed that the F-actin stabilization occurs at a faster rate than published measures on increase in PSD proteins concentrations[5,12]. Further experiments are needed to test whether this is true in the spine.

Discussion

We exploited a mathematical model of dendritic spines to test various hypotheses regarding the role and distribution of F-actin polymerization after induction of LTP. Our model operates in a physiological temporal and spatial regime; however, an exact fitting would require additional experimental data, which are currently not available. We adopted a framework where we considered membranes as a two-dimensional elastic continuum[26] without accounting for lipid dynamics[27]. Moreover, we implemented a continuous force generated by actin polymerization rather than simulating the stochastic dynamics of actin[10,25,28]. With this framework, we were able to quantify spine enlargement and local membrane tension force. Unlike other 3D models of dendritic spines[19,29], our model allows for asymmetries that prove to be crucial for membrane properties, such as the force generated by the membrane tension.

Our results indicate that F-actin polymerization increases the force generated by membrane tension and that such an increase is faster for a single focus of polymerization of actin filaments within the spine than for a spine with multiple foci. Moreover, this force is higher if the focus is located near the PSD. Since membrane tension serves as a signal for exocytosis[15], these results are in line with experimental data that show a specialized zone near the PSD for exocytosis of recycling endosomes containing glutamate receptors[22]. These experiments demonstrate that exocytosis is abrupt and massive, and it occurs in an all-or-non fashion in a zone defined by t-SNARE syntaxin 4[22], but they did not investigate the effects on membrane tension. However, Kliesch et al. showed that membrane fusion efficiency mediated by SNARE proteins increases with membrane tension[14] and Grafmüller et al. suggested that tension has to increase to start vesicle fusion[30]. Therefore, we propose that t-SNARE syntaxin 4 and an increase in membrane tension, due to actin polymerization, have to co-locate to trigger exocytosis in spines.

Each step of exocytosis is aided by the actin cytoskeleton in different ways[31]. Actin also executes different functions depending on the vesicle size, which dictates the duration of the exocytotic event[31]. Here, instead of modeling all the exocytotic phases, we investigated whether actin polymerization induces a full merge of the Ω-profile. Since exocytosis allows the membrane to achieve spine enlargement[23], this full merge is important. We found that, indeed, surface area and volume increase when actin polymerization is present. Further studies could consider a more detailed description of the force performed by actin filaments, like in previous studies of endocytosis[32]. Although endocytosis of AMPAr plays a central role in long term depression (LTD)[33] and synaptic scaling[34], we did not consider it for this study because it does not play a role in spine enlargement upon LTP induction.

Our model shows that the F-actin pool responsible for increasing the spine size and the force generated by the membrane tension also promotes full merge of the Ω-profile. Therefore, we investigated whether this pool could account for spine stabilization when it is not longer polymerizing at a fast rate. For this, we assumed that F-actin slowly stabilizes and serves as a scaffold for proteins and receptors at the PSD. We found that without this mechanism, the spine shrinks to its original size. Therefore, the here-proposed F-actin pool, that needs to polymerize at a single location close to the PSD to elevate the membrane tension and trigger exocytosis, acts as the "enlargement pool" proposed by Honkura et al.[8]. Furthermore, this actin may act as a synaptic "tag" that captures newly synthesized LTP-related proteins[35,36].

In conclusion, using our model we were able to investigate in detail the relationship between cell morphology, mechanical properties and LTP-induced events in the dendritic spines. This is a first step towards an in sillico structural model of LTP, that can be extended to include a more accurate description of actin filaments and lipid dynamics. Moreover, further work can link to AMPAR dynamics[37,38].

Methods

Model. Following our previous work[10], we use a 3D mesh of $n_{vertices}$ vertices at positions $\mathbf{x}^k = (x^k, y^k, z^k) \in \mathbb{R}^3$, $k \in \{1, 2, 3, \ldots, n_{vertices}\}$ to represent the spine membrane. At each time-step Δ_t, the vertices move according to

$$\frac{d\mathbf{x}^k}{dt} = \zeta \left(\mathbf{F}_{mem}(\mathbf{x}^k) + \mathbf{F}_{actin}(\mathbf{x}^k) \right), \tag{1}$$

where $\mathbf{F}_{actin}$ is the force generated by F-actin polymerization, given by

Symbol	Unit	Definition	Value	Source
Δ_t	s	Length of the time-step	1/8	[10]
r_s	μm	Initial spine radius	0.4	To match measures in[20]
r_{neck}	μm	Neck radius	0.0796	[20]
r_{PSD_0}	μm	Initial PSD radius	0.1744	To match measures in[20]
h_{neck}	μm	Value for fixing the neck	− 0.3920	Calculated as in[10]
h_{PSD}	μm	Value for fixing the PSD	0.36	Calculated as in[10]
P	pN μm^{-2}	Difference between internal and external pressure	75	Calculated as in[10]
σ	pN μm^{-1}	Surface tension	15	[10]
κ	pN μm	Bending modulus	0.18	[10]
α	pN	Strength of filament influence	3.8	[10]
ζ	μm^2 s^{-1} pN^{-1}	Strength of force update	0.004	[10]
n_{fil}	1	Number of actin filaments in the spine head	70	[29]
δ_s	μm	Target length of an edge	0.03	[10]
Δ_{PSD}	μm s^{-1}	PSD increasing rate	$\delta_s/60$	–

Table 1. Model parameter values.

$$\mathbf{F}_{actin}\left(\mathbf{f}^i, \mathbf{x}^k\right) = \frac{\alpha\phi(n_f)}{d\left(\mathbf{f}^i, \mathbf{x}^k\right)}\mathbf{V}_{(\mathbf{f}^i,\mathbf{x}^k)}, \tag{2}$$

with $d(\mathbf{f}^i, \mathbf{x}^k)$ representing the distance between the ith actin polymerization focus initial position $\mathbf{f}^i$ and the kth mesh vertex $\mathbf{x}^k$. We assume that F-actin extends and branches from this location. Here, $\mathbf{V}_{(\mathbf{f}^i,\mathbf{x}^k)}$ is the normalized direction vector from the focus to the mesh vertex, α is the strength of F-actin influence and $\phi(n_f) = \frac{n_{fil}}{n_{vertices_0} n_f}$ is a constant proportional to the number of F-actin n_{fil} observed experimentally[29] and inversely proportional to the number of actin nucleation locations n_f and the number of vertices of the "resting shape" $n_{vertices_0}$ (in black, Fig. 2a). In this work, we use the same "resting shape" for initiating all simulations, hence, $n_{vertices_0}$ does not vary. This quantity is reported to allow numerical accuracy when working with different choices of "resting shape" meshes due to a change in δ_s or spine size.

In Eq. (1), ζ is the strength of force update and $\mathbf{F}_{mem}$ is the force generated by the membrane, given by

$$\mathbf{F}_{mem}\left(\mathbf{x}^k\right) = -\frac{\partial \mathcal{E}_{mem}}{\partial \mathbf{x}^k}, \tag{3}$$

where

$$\mathcal{E}_{mem} = P \oint \mathrm{d}V + \sigma \oint \mathrm{d}A + 2\kappa \oint \mathrm{d}H^2 \tag{4}$$

represents the membrane energy. Here, P is the difference between internal and external pressure, V the volume, σ the surface tension, A the surface area, κ the bending modulus, and H the mean curvature. P, σ and κ are constant parameters that depend on the cell type[39]. The last term of Eq. (4) corresponds to the bending energy, described by Helfrich[40–42], which increases when the membrane is deformed and induces forces that return the membrane to its resting shape. The first and second term in Eq. (4) correspond to the volume and surface area constrains, respectively. The arrows in Fig. 2a show how these forces act in the spine membrane. See Bonilla-Quintana et al.[10] for details of the calculations.

Implementation. As in Bonilla-Quintana et al.[10], we run the simulations in MATLAB on a desktop computer. At each time-step, Eq. (1) is solved using a classical Runge–Kutta algorithm. Importantly, for numerical accuracy, the mesh has to be isotropic and conserve the number of neighbors of each vertex. Hence, remeshing is needed. For this we use the `remeshing.m` function[43], that is based on Openmesh[44], with three iterations and a target length of δ_s. Parameters for the simulation are given in Table 1. Most of the parameters in Table 1 correspond to those used in our previous work[10] which are "as discussed there" based on experimental observations. The others are calculated or set to match the modeled spine in the current work to the existing data, too, as far as possible.

The resting shape (black mesh in Fig. 2a) is found as in Bonilla-Quintana et al.[10]. In short, from a sphere with radius r_s, the points corresponding to the neck and PSD are fixed to h_{neck} and h_{PSD}, respectively, and $\mathbf{F}_{actin}$ is set to $\mathbf{0}$. We let the shape evolve until it settles. In this resting shape, the tracking points are selected to be isotropic with edge length $2\delta_s$. At each time-step, each term of $\mathbf{F}_{mem}$ (Eq. 3) is calculated for these points. Particularly, for each tracking point $\mathbf{x}^j$, the force generated by the membrane tension is given by $-\frac{\partial}{\partial \mathbf{x}^j}\left(\sigma \oint \mathrm{d}A\right)$. Therefore, our measure of the force generated by tension is equivalent to the mechanical work needed to increase the surface

area of the spine. To compare the force generated at different locations, we take its norm $||\cdot||$. The location of the F-actin polymerization foci are selected by either choosing a vertex of the resting shape and scale it 99% or by remeshing a scaled version of the resting shape (99%) with a larger vertex length. This way, the foci are equally distributed within the spine.

The Ω-profile formed during exocytosis is generated by displacing the nearest mesh vertex to the tracking point with higher tension towards the spine center. Then, the neighboring vertices are arranged to form a sphere-like shape with a resulting diameter of $\approx 0.125\,\mu m$ that is within the physiological regime (30–300 nm) reported by Wen et al.[16]. Finally, vertices near to the spine surface are moved to form the Ω-profile and the spine shape is remeshed to guarantee an isotropic mesh.

For the stabilization of F-actin, at each time-step, the PSD radius increases at a rate of Δ_{PSD} and F-actin corresponding to spine enlargement within this radius is stabilized. This is done by fixing the mesh vertices that are within the increased radius in the $x-y$ coordinates with $||z - h_{PSD}|| \leq 0.001$ to a height of h_{PSD} This allows to asymmetrically fix the PSD at the locations where the spine experience growth. Selecting a larger tolerance for the z value leads to a more isotropic enlargement of the PSD.

Code availability

Custom computer code used to generate the findings of this study is publicly available in Github https://github.com/MayteBQ/3D-Spine-LTP .

Received: 23 November 2020; Accepted: 15 March 2021
Published online: 29 March 2021

References

1. Matsuzaki, M., Honkura, N., Ellis-Davies, G. C. R. & Kasai, H. Structural basis of long-term potentiation in single dendritic spines. *Nature* **429**, 761–766. https://doi.org/10.1038/nature02617 (2004).
2. Park, M., Penick, E. C., Edwards, J. G., Kauer, J. A. & Ehlers, M. D. Recycling endosomes supply AMPA receptors for LTP. *Science* **305**, 1972. https://doi.org/10.1126/science.1102026 (2004).
3. Makino, H. & Malinow, R. Ampa receptor incorporation into synapses during LTP: The role of lateral movement and exocytosis. *Neuron* **64**, 381–390. https://doi.org/10.1016/j.neuron.2009.08.035 (2009).
4. Borovac, J., Bosch, M. & Okamoto, K. Regulation of actin dynamics during structural plasticity of dendritic spines: Signaling messengers and actin-binding proteins. *Mol. Cell. Neurosci.* **91**, 122–130. https://doi.org/10.1016/j.mcn.2018.07.001 (2018).
5. Bosch, M. *et al.* Structural and molecular remodeling of dendritic spine substructures during long-term potentiation. *Neuron* **82**, 444–459. https://doi.org/10.1016/j.neuron.2014.03.021 (2014).
6. Okamoto, K.-I., Nagai, T., Miyawaki, A. & Hayashi, Y. Rapid and persistent modulation of actin dynamics regulates postsynaptic reorganization underlying bidirectional plasticity. *Nat. Neurosci.* **7**, 1104–1112. https://doi.org/10.1038/nn1311 (2004).
7. Fischer, M., Kaech, S., Knutti, D. & Matus, A. Rapid actin-based plasticity in dendritic spines. *Neuron* **20**, 847–854. https://doi.org/10.1016/S0896-6273(00)80467-5 (1998).
8. Honkura, N., Matsuzaki, M., Noguchi, J., Ellis-Davies, G. C. R. & Kasai, H. The subspine organization of actin fibers regulates the structure and plasticity of dendritic spines. *Neuron* **57**, 719–729. https://doi.org/10.1016/j.neuron.2008.01.013 (2008).
9. Frost, N. A., Shroff, H., Kong, H., Betzig, E. & Blanpied, T. A. Single-molecule discrimination of discrete perisynaptic and distributed sites of actin filament assembly within dendritic spines. *Neuron* **67**, 86–99. https://doi.org/10.1016/j.neuron.2010.05.026 (2010).
10. Bonilla-Quintana, M., Wörgötter, F., Tetzlaff, C. & Fauth, M. Modeling the shape of synaptic spines by their actin dynamics. *Front. Synaptic Neurosci.* **12**, 9. https://doi.org/10.3389/fnsyn.2020.00009 (2020).
11. Cingolani, L. A. & Goda, Y. Actin in action: The interplay between the actin cytoskeleton and synaptic efficacy. *Nat. Rev. Neurosci.* **9**, 344–356. https://doi.org/10.1038/nrn2373 (2008).
12. Meyer, D., Bonhoeffer, T. & Scheuss, V. Balance and stability of synaptic structures during synaptic plasticity. *Neuron* **82**, 430–443. https://doi.org/10.1016/j.neuron.2014.02.031 (2014).
13. Mogilner, A. & Oster, G. Cell motility driven by actin polymerization. *Biophys. J.* **71**, 3030–3045. https://doi.org/10.1016/S0006-3495(96)79496-1 (1996).
14. Kliesch, T.-T. *et al.* Membrane tension increases fusion efficiency of model membranes in the presence of snares. *Sci. Rep.* **7**, 12070. https://doi.org/10.1038/s41598-017-12348-w (2017).
15. Gauthier, N. C., Fardin, M. A., Roca-Cusachs, P. & Sheetz, M. P. Temporary increase in plasma membrane tension coordinates the activation of exocytosis and contraction during cell spreading. *Proc. Natl. Acad. Sci.* **108**, 14467. https://doi.org/10.1073/pnas.1105845108 (2011).
16. Wen, P. J. *et al.* Actin dynamics provides membrane tension to merge fusing vesicles into the plasma membrane. *Nat. Commun.* **7**, 12604. https://doi.org/10.1038/ncomms12604 (2016).
17. Xiong, Y. *et al.* Mechanisms controlling cell size and shape during isotropic cell spreading. *Biophys. J.* **98**, 2136–2146. https://doi.org/10.1016/j.bpj.2010.01.059 (2010).
18. Rangamani, P. *et al.* Signaling network triggers and membrane physical properties control the actin cytoskeleton-driven isotropic phase of cell spreading. *Biophys. J.* **100**, 845–857. https://doi.org/10.1016/j.bpj.2010.12.3732 (2011).
19. Alimohamadi, H., Bell, M. K., Halpain, S. & Rangamani, P. Mechanical principles governing the shapes of dendritic spines. *bioRxiv*. https://doi.org/10.1101/2020.09.09.290650 (2020).
20. Arellano, J., Benavides-Piccione, R., DeFelipe, J. & Yuste, R. Ultrastructure of dendritic spines: Correlation between synaptic and spine morphologies. *Front. Neurosci.* **1**, 10. https://doi.org/10.3389/neuro.01.1.1.010.2007 (2007).
21. Mogilner, A. & Edelstein-Keshet, L. Regulation of actin dynamics in rapidly moving cells: A quantitative analysis. *Biophys. J.* **83**, 1237–1258. https://doi.org/10.1016/S0006-3495(02)73897-6 (2002).
22. Kennedy, M. J., Davison, I. G., Robinson, C. G. & Ehlers, M. D. Syntaxin-4 defines a domain for activity-dependent exocytosis in dendritic spines. *Cell* **141**, 524–535. https://doi.org/10.1016/j.cell.2010.02.042 (2010).
23. Park, M. *et al.* Plasticity-induced growth of dendritic spines by exocytic trafficking from recycling endosomes. *Neuron* **52**, 817–830. https://doi.org/10.1016/j.neuron.2006.09.040 (2006).
24. Rex, C. S. *et al.* Myosin IIB regulates actin dynamics during synaptic plasticity and memory formation. *Neuron* **67**, 603–617. https://doi.org/10.1016/j.neuron.2010.07.016 (2010).
25. Bonilla-Quintana, M., Wörgötter, F., D'Este, E., Tetzlaff, C. & Fauth, M. Actin in dendritic spines self-organizes into a critical state. *bioRxiv*. https://doi.org/10.1101/2020.04.22.054577 (2020).

26. Guckenberger, A. & Gekle, S. Theory and algorithms to compute helfrich bending forces: A review. *J. Phys. Condensed Matter* **29**, 203001 (2017).
27. Dotti, C. G., Esteban, J. A. & Ledesma, M. D. Lipid dynamics at dendritic spines. *Front. Neuroanat.* **8**, 76. https://doi.org/10.3389/fnana.2014.00076 (2014).
28. Bennett, M. R., Farnell, L. & Gibson, W. G. A model of NMDA receptor control of f-actin treadmilling in synaptic spines and their growth. *Bull. Math. Biol.* **73**, 2109–2131. https://doi.org/10.1007/s11538-010-9614-4 (2011).
29. Miermans, C. A., Kusters, R. P. T., Hoogenraad, C. C. & Storm, C. Biophysical model of the role of actin remodeling on dendritic spine morphology. *PLoS One* **12**, e0170113. https://doi.org/10.1371/journal.pone.0170113 (2017).
30. Grafmüller, A., Shillcock, J. & Lipowsky, R. The fusion of membranes and vesicles: Pathway and energy barriers from dissipative particle dynamics. *Biophys. J.* **96**, 2658–2675. https://doi.org/10.1016/j.bpj.2008.11.073 (2009).
31. Porat-Shliom, N., Milberg, O., Masedunskas, A. & Weigert, R. Multiple roles for the actin cytoskeleton during regulated exocytosis. *Cell. Mol. Life Sci.* **70**, 2099–2121. https://doi.org/10.1007/s00018-012-1156-5 (2013).
32. Akamatsu, M. *et al.* Principles of self-organization and load adaptation by the actin cytoskeleton during clathrin-mediated endocytosis. *eLife* **9**, e49840. https://doi.org/10.7554/eLife.49840 (2020).
33. Beattie, E. C. *et al.* Regulation of AMPA receptor endocytosis by a signaling mechanism shared with ltd. *Nat. Neurosci.* **3**, 1291–1300. https://doi.org/10.1038/81823 (2000).
34. Turrigiano, G. G. The self-tuning neuron: Synaptic scaling of excitatory synapses. *Cell* **135**, 422–435. https://doi.org/10.1016/j.cell.2008.10.008 (2008).
35. Okamoto, K., Bosch, M. & Hayashi, Y. The roles of Camkii and f-actin in the structural plasticity of dendritic spines: A potential molecular identity of a synaptic tag?. *Physiology* **24**, 357–366. https://doi.org/10.1152/physiol.00029.2009 (2009).
36. Frey, U. & Morris, R. G. M. Synaptic tagging and long-term potentiation. *Nature* **385**, 533–536. https://doi.org/10.1038/385533a0 (1997).
37. Kusters, R., Kapitein, L. C., Hoogenraad, C. C. & Storm, C. Shape-induced asymmetric diffusion in dendritic spines allows efficient synaptic AMPA receptor trapping. *Biophys. J.* **105**, 2743–2750. https://doi.org/10.1016/j.bpj.2013.11.016 (2013).
38. Becker, M. F. P. & Tetzlaff, C. The biophysical basis underlying the maintenance of early phase long-term potentiation. *bioRxiv*. https://doi.org/10.1101/2020.08.12.247726 (2020).
39. Pontes, B. *et al.* Membrane elastic properties and cell function. *PLoS One* **8**, e67708. https://doi.org/10.1371/journal.pone.0067708 (2013).
40. Helfrich, W. Elastic properties of lipid bilayers: Theory and possible experiments. *Zeitschrift für Naturforschung C* **28**, 693–703. https://doi.org/10.1515/znc-1973-11-1209 (1973).
41. Doubrovinski, K. & Kruse, K. Cell motility resulting from spontaneous polymerization waves. *Phys. Rev. Lett.* **107**, 258103. https://doi.org/10.1103/PhysRevLett.107.258103 (2011).
42. Guckenberger, A., Schraml, M. P., Chen, P. G., Leonetti, M. & Gekle, S. On the bending algorithms for soft objects in flows. *Comput. Phys. Commun.* **207**, 1–23. https://doi.org/10.1016/j.cpc.2016.04.018 (2016).
43. Helf, C. Matlab isotropic remesher. https://github.com/christopherhelf/isotropicremeshing/blob/master/README.md. GitHub, Inc (2015). Retrieved November 20 (2018).
44. Botsch, M., Steinberg, S., Bischoff, S. & Kobbelt, L. Openmesh—A generic and efficient polygon mesh data structure (2002).
45. Bonilla-Quintana, M. & Woergoetter, F. Exploring new roles for actin upon ltp induction in dendritic spines. *bioRxiv*. https://doi.org/10.1101/2020.11.14.382663 (2020).

Acknowledgements

We thank the German Science Foundation through the Collaborative Research Center SFB-1286, Project C3 for funding this research. This paper has been previously posted on bioRxiv[45].

Author contributions

M.B.-Q. performed research and wrote the first draft. M.B.-Q. and F.W. contributed to the study concept. F.W. edited the paper.

Funding

Open Access funding enabled and organized by Projekt DEAL.

Competing interests

The authors declare no competing interests.

Additional information

Supplementary Information The online version contains supplementary material available at https://doi.org/10.1038/s41598-021-86367-z.

Correspondence and requests for materials should be addressed to M.B.-Q.

Reprints and permissions information is available at www.nature.com/reprints.

Publisher's note Springer Nature remains neutral with regard to jurisdictional claims in published maps and institutional affiliations.